Inorganic Chemistry

Article

pubs.acs.org/IC

Selective and Reversible Base-Induced Elimination of a Ruthenium Dithioether Yields a Vinyl Metallosulfonium Complex

Rajat Chauhan, Mark S. Mashuta, and Craig A. Grapperhaus*

Department of Chemistry, University of Louisville, 2320 South Brook Street, Louisville, Kentucky 40292, United States

Supporting Information

ABSTRACT: Chemical oxidation of tris(2-diphenylphosphinebenzenethiolato)ruthenate(II) $[\mathbf{Ru\text{-}1}]^-$ with ferrocenium hexafluorophosphate in the presence of ethylene yields [(2-diphenylphosphinebenzenethiolato)(ethane-1,2-diylbis(thio-2,1-phenylene)diphenylphosphine)ruthenium(II)] hexafluorophosphate, $[\mathbf{Ru\text{-}1{\cdot}C_2H_4}]\mathbf{PF_6}$, from addition of the alkene across cis sulfur sites. The $[\mathbf{Ru\text{-}1{\cdot}C_2H_4}]^+$ complex displays a single redox couple at +794 mV versus ferrocenium/ferrocene. ^{1}H NMR of $[\mathbf{Ru\text{-}1{\cdot}C_2H_4}]^+$ displays ethylene resonances at δ = 1.29 (td, 1H), 1.59 (td, 1H), 2.78 (dd, 1H), and 3.03 (dd, 1H). In the presence of base $[\mathbf{Ru\text{-}1{\cdot}C_2H_4}]^+$ is selectively deprotonated at the pseudoequatorial proton on the carbon α to the sulfur trans to phosphorus, yielding the vinyl metallosulfonium derivative $[\mathbf{Ru\text{-}1{\cdot}C_2H_3}]$. ^{1}H and ^{31}P NMR spectra of $[\mathbf{Ru\text{-}1{\cdot}C_2H_3}]$ are temperature dependent, associated with inversion of the sulfur lone pair at the vinyl metallosulfonium. The activation energy for the fluxional process calculated using density functional theory (B3LYP/LANL2DZ+6-31g) of 14.36 kcal/mol is consistent with the experimentally determined value of 13.08 kcal/mol. The complex $[\mathbf{Ru\text{-}1{\cdot}C_2H_3}]$ crystallizes as yellow blocks in the triclinic space group *P*-1 with unit cell dimensions of a = 11.2718(5) Å, b =12.0524(3) Å, c = 23.6075(10) Å, α = 101.715(3)°, β = 98.154(4)°, and γ = 105.209(3)°. Addition of hydrochloric acid to $[\mathbf{Ru\text{-}1{\cdot}C_2H_3}]$ regenerates $[\mathbf{Ru\text{-}1{\cdot}C_2H_4}]^+$. Addition of DCl confirms the selectivity of this reverse reaction.

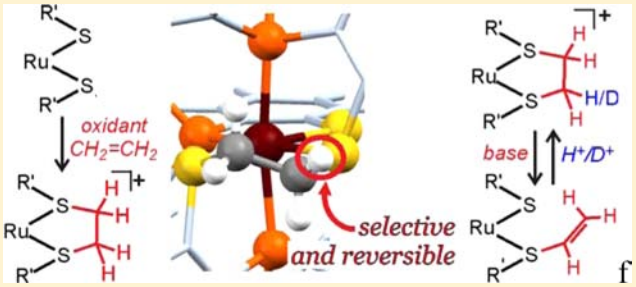

INTRODUCTION

Base-induced elimination of organic trialkyl sulfoniums (R_3S^+) to yield alkenes and sulfides is well known, Scheme 1.[1]

Scheme 1. Base-Induced Eliminations

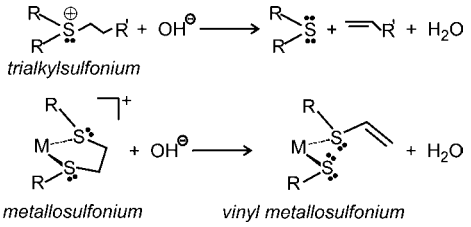

Similarly, metal coordination of thioethers imparts partial sulfonium character on the sulfur donor, leading to base sensitivity of the resulting "metallosulfonium complex". Several cationic metal–dithioether complexes with five-membered chelate structures readily undergo base-induced elimination, yielding metal complexes with one thiolate and one vinyl substituent, Scheme 1.[2−6] The resulting vinyl metallosulfonium complexes are susceptible to further reactivity. Examples include the *reversible* deprotonation/protonation of $[Co(TTCN)_2]^{3+}$ with a pK_a near 4.0 in aqueous solution by Blake et al.[3] and the intramolecular C–C coupling between a C_6Me_6 ring and the vinyl sulfide in the presence of excess base reported by Goh and Webster.[5] In the current manuscript, we report the selective deprotonation/protonation and reactivity of a cationic metal–dithioether complex prepared by oxidation-induced alkene addition to a metal–thiolate precursor.

The carbon–sulfur bond forming reaction between organic thiyl radicals and alkenes is well established with applications including cis/trans isomerization, sulfide synthesis, and polymerization.[7−10] Similar reactions have been reported between oxidized metal–sulfur complexes including metal dithiolenes[11−16] and metal–thiolates.[17−22] The former has been known since the 1960s,[12] although the report of reversible ethylene addition to nickel–dithiolenes by Wang and Stiefel renewed interest in these complexes.[11] The promise of these complexes in ethylene purification was never realized due in large part to complications arising from deleterious interligand addition, which is favored over the initially reported intraligand product. Recent elegant studies by Fekl detailed the necessity for an anionic, reduced metal complex in the reaction mixture to obtain the latter.[13] In related studies, Fekl also noted oxidation-induced addition of ethylene to a Mo tris(dithiolene)[14] and dienes to Pt bis(dithiolene).[16]

Our studies focused on the trischelate complexes $[Ru(DPPBT)_3]^-$, $[\mathbf{Ru\text{-}1}]^-$, and $Re(DPPBT)_3$, **Re-1** (DPPBT =

Received: May 11, 2012
Published: June 29, 2012

   dx.doi.org/10.1021/ic300983x | *Inorg. Chem.* 2012, 51, 7913−7920

diphenylphosphinobenzenethiolate), which precludes intraligand addition and orients two of the thiolate donors in a position that favors interligand addition, Scheme 2. Oxidation

Scheme 2. Ligand-Centered Reactivity of [Ru-1]$^-$ and Its Derivatives

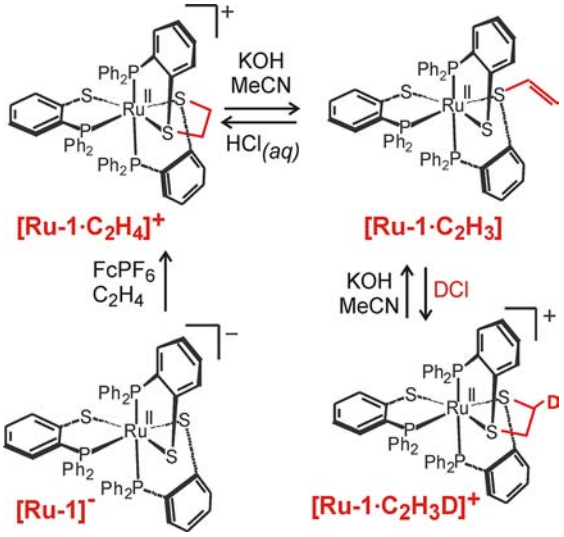

of [**Ru-1**]$^-$ to the formally Ru(IV) derivative [**Ru-1**]$^+$ results in a significant increase in spin density on the sulfur donors, leading to our assignment of the complex as a metal-stabilized thiyl radical.[21,23] The [**Ru-1**]$^+$ complex readily reacts with alkenes,[18−20] methyl ketones,[24] and alkynes[17] across the cis-sulfur sites to yield isolable metal−thioether complexes. The rate of alkene addition is fastest for electron-donating alkenes, consistent with an electrophilic metal-stabilized thiyl radical.[18] While the reaction is irreversible for [**Ru-1**]$^+$, reversible ethylene addition was observed for the Re derivative, [**Re-1**]$^+$.[19]

In our prior studies we established the addition of a variety of alkenes to [**Ru-1**]$^+$ by electrochemical methods.[20] However, few of these complexes have been prepared on a synthetic scale and isolated for further reactivity studies. In the current article, we report the synthesis of the ethylene addition product [**Ru-1·C_2H_4**]$^+$ by chemical methods and explore its acid/base chemistry in solution, Scheme 2. The complex has previously been prepared by nucleophilic addition of 1,2-dibromoethane to the anionic complex [**Ru-1**]$^-$.[20] However, this route is only accessible for products with readily available dihaloalkane precursors, whereas the methods reported herein are applicable to a variety of alkenes including styrenes as previously reported.[18] In the presence of base, [**Ru-1·C_2H_4**]$^+$ is selectively deprotonated to the vinyl metallosulfonium derivative [**Ru-1·C_2H_3**]. Addition of acid reverses the reaction. This reaction represents an initial survey of the reactivity of vinyl metallosulfonium complexes, which may have relevance for the functionalization of olefins via ligand-centered reactivity.

EXPERIMENTAL SECTION

Materials and Reagents. All reagents were obtained from commercially available sources and used as received unless otherwise noted. All solvents were dried and freshly distilled using standard techniques under a nitrogen atmosphere and degassed using the freeze−pump−thaw method. Reactions were conducted using standard Schlenk techniques under a nitrogen atmosphere or in an argon-filled glovebox unless otherwise noted. The complex $HNEt_3$[**Ru-1**] was prepared according to methods previously reported by Dilworth et al.[25] The complex [**Ru-1·C_2H_4**]PF_6 was previously observed upon electrochemical oxidation of PPN[**Ru-1**] in the presence of ethylene.[20]

[Ru-1·C_2H_4][PF_6]. In an ice bath at 0 °C a yellow solution of $HNEt_3$[**Ru-1**] (100 mg, 0.0935 mmol) in acetonitrile (40 mL) was saturated with ethylene gas by purging the solution via syringe for 3−5 min. A blue solution of ferrocenium hexafluorophosphate (0.0619 g, 0.187 mmol) in acetonitrile (30 mL) was added by cannula transfer. The resulting green solution was stirred for 3 h at 0 °C followed by removal of solvent by rotary evaporation. The crude yellow−green residue was washed with an excess of hot water (300 mL) and diethyl ether (25 mL). The product is spectroscopically identical to the previously reported derivative.[20] Yield: 0.065 g (60%). $E_{1/2}$ vs Fc^+/Fc (Ru^{III}/Ru^{II}) = +794 mV. ^{1}H NMR (500 MHz, CD_3CN): δ 1.29 (td, 1H, J = 14, 14, 4 Hz, $SCHH_{ax}CH_2S$), 1.59 (td, 1H, J = 14, 14, 4 Hz, $SCH_2CHH_{ax}S$), 2.78 (dd, 1H, J = 14, 4 Hz, $SCH_2CHH_{eq}S$), 3.03 (dd, 1H, J = 14, 4 Hz, $SCHH_{eq}CH_2S$), 6.32−8.29 (m, 42H, $SC_6H_4P(C_6H_5)_2$). Selected $^{13}C\{^1H\}$ NMR (176 MHz, CD_3CN): δ 36.2 (s, SCH_2CH_2S), 44.2 (s, SCH_2CH_2S). $^{31}P\{^1H\}$ NMR (162 MHz, CD_3CN): δ 40.3 (J = 30, 304 Hz, P_{ax1}) 37.5 (J = 30, 304 Hz, P_{ax2}), 61.0 (J = 30, 30 Hz, P_{eq}).

[Ru-1·C_2H_3]. To a yellow-green solution of [**Ru-1·C_2H_4**][PF_6] (100 mg, 0.087 mmol) in acetonitrile (40 mL) was added an 0.18 M solution of KOH in methanol (0.49 mL, 0.087 mmol). The resulting solution was stirred for 30 min, during which time the color changed to golden yellow. Solvent was removed by rotary evaporation to yield a yellow residue. The crude product was washed with an excess of water (300 mL). Yield: 0.084 g (96%). X-ray quality crystals were obtained by addition of 30 mg of crude product to 3 mL of toluene. Slow evaporation yielded golden yellow crystals. $E_{1/2}$ vs Fc^+/Fc (Ru^{III}/Ru^{II}) = −250 mV. +ESI-MS for $RuP_3S_3C_{56}H_{45}$, $[M + H]^+$ 1009.0978 found, 1009.1018 calcd. Anal. Calcd for $RuP_3S_3C_{56}H_{45}\cdot C_8H_7$: C, 68.77; H, 4.86. Found: C, 68.22; H, 4.77. ^{1}H NMR (500 MHz, CD_3CN): δ 4.01 (d, 1H, J = 16 Hz, $SCH{=}CHH_{cis}$), 4.40 (d, 1H, J = 9 Hz, $SCH{=}CHH_{trans}$), 4.94 (dd, 1H, J = 16, 9 Hz, $SCH{=}CH_2$), 6.32−8.29 (m, 42H, $SC_6H_4P(C_6H_5)_2$). Selected $^{13}C\{^1H\}$ NMR (176 MHz, CD_3CN): δ 120.0 (s, $SCH{=}CH_2$). $^{31}P\{^1H\}$ NMR (162 MHz, CD_3CN): δ 55.4 (J = 30, 310 Hz, P_{ax1}) 48.7 (J = 30, 310 Hz, P_{ax2}), 58.3 (J = 30, 30 Hz, P_{eq}).

[Ru-1·C_2H_3D]Cl. To a golden yellow solution of [**Ru-1·C_2H_3**] (100 mg, 0.099 mmol) in benzene (10 mL) was added a 35% solution of DCl in D_2O (9.57 μL, 0.099 mmol). The resulting solution was heated at reflux for 1 h, during which time the color changed to chartreuse yellow. Solvent was removed by rotary evaporation to yield a yellow-green residue. The crude product was washed with an excess of water (300 mL) and diethyl ether (25 mL). Yield: 0.093 g (90%). $E_{1/2}$ vs Fc^+/Fc (Ru^{III}/Ru^{II}) = +794 mV. +ESI-MS for $C_{56}H_{45}DP_3S_3Ru$: $[M]^+$ 1010.1104 found, 1010.1081 calcd. ^{1}H NMR (500 MHz, CD_3CN): δ 1.29 (t, 1H, J = 14, 14 Hz, $SCHH_{ax}CHDS$), 1.59 (dd, 1H, J = 14, 4 Hz, $SCH_2CDH_{ax}S$), 3.03 (dd, 1H, J = 14, 4 Hz, $SCHH_{eq}CHDS$), 6.32−8.29 (m, 42H, $SC_6H_4P(C_6H_5)_2$). Selected $^{13}C\{^1H\}$ NMR (176 MHz, CD_3CN): δ 35.8 (t, J_{CD} = 20.4 Hz, SCH_2CHDS), 44.2 (s, SCH_2CHDS). $^{31}P\{^1H\}$ NMR (162 MHz, CD_3CN): δ 40.3 (J = 30, 304 Hz, P_{ax1}) 37.5 (J = 30, 304 Hz, P_{ax2}), 61.0 (J = 30, 30 Hz, P_{eq}).

Physical Methods. Mass spectra were collected by the Mass Spectrometry Application and Collaboration Facility in the Chemistry Department at Texas A&M University. Elemental analyses were performed by Midwest Microlab (Indianapolis). All electrochemical measurements were performed using a PAR 273 potentiostat/galvanostat with a three-electrode cell (glassy carbon working electrode, platinum wire counter electrode, and Ag/Ag ion reference electrode). Reported potentials are scaled versus a ferrocenium/ferrocene (Fc^+/Fc) standard (0.00 V), which was determined using ferrocene as an internal standard. ^{1}H NMR and gCOSY spectra, referenced to TMS, were recorded on a Varian 500 MHz spectrometer. ^{31}P NMR spectra were recorded on a Varian 400 MHz spectrometer and are referenced to 85% H_3PO_4. ^{13}C and gHSQCAD NMR spectra were recorded on a Varian 700 MHz spectrometer. The activation energy ($\Delta G^\dagger$) for the fluxional NMR process was calculated using the following equation[26]

dx.doi.org/10.1021/ic300983x | Inorg. Chem. 2012, 51, 7913−7920

$$\Delta G^{\ddagger} = aT[9.972 + \log(T_c/\Delta\nu)]$$

where $a = 4.575 \times 10^{-3}$ kcal/mol, T_c = coalescence temperature, and $\Delta\nu$ = frequency difference at the low-temperature limit.

Crystallographic Stuides. A yellow block crystal of [**Ru-1·C_2H_3**] was cut to dimensions 0.25 × 0.13 × 0.10 mm^3 and mounted on a glass fiber for collection of X-ray data on an Agilent Technologies/Oxford Diffraction Gemini CCD diffractometer. The CrysAlisPro[27] CCD software package (v 171.35.11) was used to acquire a total of 913 30-s frame ω-scan exposures of data at 100(1) K to a $2\theta_{max}$ = 59.20° using monochromated Mo Kα radiation (0.71073 Å) from a sealed tube. Frame data were processed using CrysAlisPro[27] RED to determine final unit cell parameters: a = 11.2718(5) Å, b = 12.0524(3) Å, c = 23.6075(10) Å, α = 101.715(3)°, β = 98.154(4)°, γ = 105.209(3)°, V = 2965.04(21) $Å^3$, D_{calcd} = 1.383 Mg/m^3, Z = 2 to produce raw hkl data that were corrected for absorption (transmission min/max = 0.926/0.952; μ = 0.496 mm^{-1}) using SCALE3 ABSPACK.[28] The structure was solved by Patterson methods in the space group P-1 using SHELXS-90[29] and refined by least-squares methods on F^2 using SHELXL-97[29] incorporated into the SHELXTL[30] (v 6.14) suite of programs. The disordered toluene solvent was modeled with a one-half occupancy set of carbon atoms (C80−C86) using an appropriate set of constraints; the second set of one-half occupancy carbon atoms (C80a−C86a) involved in the disorder is generated by symmetry through an inversion center. All other non-hydrogen atoms were refined with anisotropic atomic displacement parameters. The three hydrogen atoms (H55, H56a, and H56b) of the vinyl group were located by difference maps and refined isotropically. Remaining hydrogen atoms were placed in their geometrically generated positions and refined as a riding model. Phenyl H's were included as fixed contributions with $U(H) = 1.2U_{11}$ (attached C atom), while methyl groups were allowed to ride (the torsion angle which defines its orientation was allowed to refine) on the attached C atom, and these atoms were assigned $U(H) = 1.5U_{11}$. For 12 354 reflections $I > 2\sigma(I)$ [R(int) 0.040] the final anisotropic full matrix least-squares refinement on F^2 for 735 variables converged at R1 = 0.038 and wR2 = 0.076 with a GOF of 1.04. Crystal data and structure refinement parameters for [**Ru-1·C_2H_3**] are provided in Table 1. Selected bond distances and bond angles are listed in Table 2.

Computational Methodology. Geometry optimization and frequency calculations for all complexes were performed using the Gaussian 09 suite of programs.[31] Density functional theory (DFT) calculations employed the B3LYP functional. For these calculations the 6-31g basis set was used for carbon, hydrogen, sulfur, and phosphorus atoms, while the LANL2DZ basis set was used for ruthenium. Input coordinates were taken from crystallographic data for the neutral complex [**Ru-1·C_2H_3**]. Optimized coordinates for [**Ru-1·C_2H_3**], its structural isomer, and their truncated derivates are provided in Tables S1−S6, Supporting Information. To investigate the rotation and inversion of the vinyl group, the Ru−S2−C55−C56 and Ru−S2−C19−C55 torsion angles were frozen, respectively, at various positions and the structure reoptimized.

RESULTS AND DISCUSSIONS

Synthesis and Characterization. A series of complexes has been prepared through successive ligand-centered reactions based on the tris(diphenylphosphinobenzenethiolato) (DPPBT) metal complex [**Ru-1**]$^-$, Scheme 2. The dithioether complex [**Ru-1·C_2H_4**]$^+$ can be prepared in 60% yield upon chemical oxidation of [**Ru-1**]$^-$ with two equivalents of ferrocenium hexafluorophosphate ($FcPF_6$) in the presence of ethylene. Deprotonation of [**Ru-1·C_2H_4**]$^+$ with KOH in acetonitrile yields the vinyl metallosulfonium derivative [**Ru-1·C_2H_3**] in an elimination reaction in 96% yield. A single structural isomer with the vinyl substituent on the sulfur trans to phosphorus is obtained. The reaction does not proceed under aqueous conditions and in basic methanolic solutions, consistent with the greater basicity of hydroxide in acetonitrile as compared to hydrogen-bonding solvents.[32,33] Acidification of [**Ru-1·C_2H_3**] with HCl or HBr regenerates [**Ru-1·C_2H_4**]$^+$.

Table 1. Crystal Data and Structure Refinement for [Ru-1·C_2H_3]·2.5 C_7H_8

empirical formula	$C_{73.50}H_{61}P_3RuS_3$
fw	1234.38
temp.	100.1 K
wavelength	0.7107 Å
cryst syst	triclinic
space group	P-1
unit cell dimens	a = 11.2718(5) Å
	b = 12.0524(3) Å
	c = 23.6075(10) Å
	α = 101.715(3)°
	β = 98.154(4)°
	γ = 105.209(3)°
vol.	2965.04(21) $Å^3$
Z	2
density (calcd)	1.383 Mg/m^3
abs coeff	0.496 mm^{-1}
F(000)	1278
cryst color, habit	yellow cut-block
cryst size	0.25 × 0.13 × 0.10 mm^3
theta range for data collection	3.37−29.62°
index ranges	$-15 \le h \le 14$, $-16 \le k \le 15$, $-31 \le l \le 31$
reflns collected	67 874
indep reflns	15 439 [R(int) = 0.041]
completeness to theta = 29.62°	92.4%
completeness to theta = 27.04°	99.8%
abs corr	semiempirical from equivalents
max/min transmission	0.952/0.926
refinement method	full-matrix least-squares on F^2
data/restraints/parameters	15439/7/735
goodness-of-fit on F^2	1.043
final R indices [$I > 2\sigma(I)$][a]	R1 = 0.0383, wR2 = 0.0763
R indices (all data)	R1 = 0.0562, wR2 = 0.0849
largest diff. peak and hole	0.763 and −0.736 e.$Å^{-3}$

[a] $R1 = \Sigma||F_o| - |F_c||/\Sigma|F_o|$. $wR2 = \{\Sigma[w(F_o^2 - F_c^2)^2]/\Sigma[w(F_o^2)^2]\}^{1/2}$, where $w = q/\sigma^2(F_o^2) + (qp)^2 + bp$. GOF = $S = \{\Sigma[w(F_o^2 - F_c^2)^2]/(n - p)\}^{1/2}$, where n is the number of reflections and p is the number of parameters refined.

Table 2. Selected Bond Distances (Angstroms) and Angles (degrees) for [Ru-1·C_2H_4]$^+$[20] and [Ru-1·C_2H_3]

	[Ru-1·C_2H_4]$^+$	[Ru-1·C_2H_3]	
	experimental	experimental	computational
Ru−S1	2.3856(9)	2.3932(5)	2.503
Ru−S2	2.3749(9)	2.4014(5)	2.541
Ru−S3	2.3365(9)	2.3992(5)	2.515
Ru−P1	2.3648(9)	2.3440(6)	2.455
Ru−P2	2.3965(10)	2.3640(6)	2.488
Ru−P3	2.3290(9)	2.2853(5)	2.409
S2−C55	1.836(4)	1.787(2)	1.864
S3−C56	1.843(4)		
C55−C56	1.510(5)	1.313(4)	1.332
S1−Ru−S2	87.06(3)	95.030(18)	93.048
S1−Ru−S3	173.73(3)	178.19(2)	176.796
S2−Ru−P3	172.87(3)	171.59(2)	173.048
P1−Ru−P2	168.81(3)	168.455(18)	167.143
Ru−S2−C55	104.52(12)	112.23(8)	111.325

dx.doi.org/10.1021/ic300983x | Inorg. Chem. 2012, 51, 7913−7920

The vinyl metallosulfonium product [**Ru-1**·C_2H_3] is easily distinguished from its dithioether precursor [**Ru-1**·C_2H_4]$^+$ by changes in color, solubility, and redox potential. The golden-yellow, neutral [**Ru-1**·C_2H_3] has enhanced solubility in nonpolar solvents, such as benzene and toluene, as compared to the chartreuse yellow, cationic precursor [**Ru-1**·C_2H_4]$^+$. The vinyl metallosulfonium complex displays a [**Ru-1**·C_2H_3]$^{+/0}$ redox couple at −250 mV versus Fc^+/Fc, Figure 1. This formal

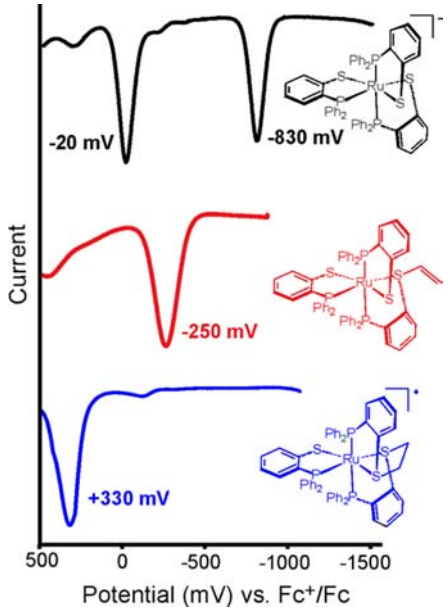

Figure 1. Square wave voltammograms of [**Ru-1**]$^-$ (top), [**Ru-1**·C_2H_3] (center), and [**Ru-1**·C_2H_4]$^+$ (bottom) in dichloromethane or acetonitrile with 0.1 M tetrabutylammonium hexafluorophosphate as supporting electrolyte. Potentials referenced to Fc^+/Fc using an internal standard.

$Ru^{III/II}$ potential is exactly centered between those previously reported for [**Ru-1**·C_2H_4]$^{2+/+}$ at +330 mV and [**Ru-1**]$^{0/-}$ at −830 mV. The results are consistent with a large (+580 mV) cathodic shift upon substitution of an anionic thiolate donor with a neutral thioether.[34] Cyclic voltammetry of [**Ru-1**·C_2H_3] confirms the oxidation is quasi-reversible with a peak-to-peak potential difference, ΔE_p, of 80 mV at a scan rate of 100 mV/s, Figure S3, Supporting Information. The two products cannot be discriminated by +ESI-MS. The dithioether complex [**Ru-1**·C_2H_4]$^+$ displays an m/z 1009.1015 amu consistent with the theoretical value of 1009.1018 amu for the M^+ ion. The vinyl complex [**Ru-1**·C_2H_3] displays a similar peak at 1009.0978 with the same theoretical value for the $[M + H]^+$ ion.

Reversible deprotonation of the ethylene linker in [**Ru-1**·C_2H_4]$^+$ proceeds selectively at the carbon alpha to the sulfur trans to phosphorus. Deuteration of [**Ru-1**·C_2H_3] with DCl yields the monodeuterated dithioether complex [**Ru-1**·C_2H_3D]$^+$, which displays an m/z peak in the +ESI-MS at 1010.1104, which is shifted by 1.0089 relative to [**Ru-1**·C_2H_4]$^+$. Further deprotonation of [**Ru-1**·C_2H_3D]$^+$ regenerates the vinyl metallosulfonium complex [**Ru-1**·C_2H_3] with no incorporation of deuterium. The results, corroborated by NMR investigations, indicate selective deprotonation of a single proton in the ethylene bridge. As described in the NMR section below, the reaction occurs only at the hydrogen in the pseudoequatorial position on the carbon alpha to the sulfur trans to phosphorus.

No reaction occurs upon addition of a large excess of base to solutions of [**Ru-1**·C_2H_3] in the absence of air even under prolonged reflux conditions. However, under aerobic conditions excess base induces C−S bond cleavage in both [**Ru-1**·C_2H_4]$^+$ and [**Ru-1**·C_2H_3] upon heating, Scheme 3. Depend-

Scheme 3. Aerobic Reaction of [Ru-1·C_2H_3] with Excess Base

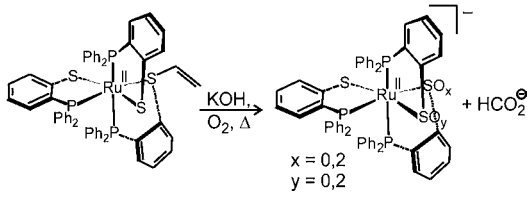

ing on the length of the reaction, [**Ru-1**]$^-$ and/or its S-oxygenated derivatives[35] are recovered as the only metal-containing products. NMR data (^1H, ^{13}C, and gHSQC; Figures S15−S17, Supporting Information) of the observed organic product are consistent with C−C bond cleavage of the ethylene bridge to yield formate. The reaction pathway remains elusive but is proposed to proceed via nucleophilic attack at the vinyl metallosulfonium under strongly basic conditions similar to observations reported by Goh and Webster.[5]

Structural Determination. Yellow block-shaped crystals of [**Ru-1**·C_2H_3] in the triclinic space group $P\bar{1}$ were obtained upon slow evaporation of toluene solution of the vinyl metallosulfonium complex. Crystal data and structure refinement details are listed in Table 1. The vinyl metallosulfonium complex [**Ru-1**·C_2H_3] contains a six-coordinated Ru(II) ion ligated by three PS chelates in a pseudo-octahedral environment as shown in the ORTEP[36] representation in Figure 2. The three sulfur donors are arranged in a meridional fashion as in related complexes.[17−20,25,37] The vinyl substituent is located at S2, which sits trans to P3. The two thiolate sulfurs, S1 and S3, are trans to each other.

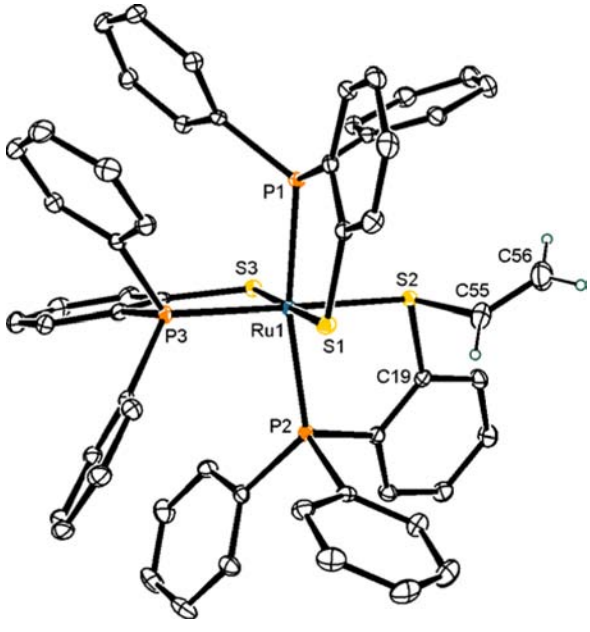

Figure 2. ORTEP[36] representation of [**Ru-1**·C_2H_3].

dx.doi.org/10.1021/ic300983x | Inorg. Chem. 2012, 51, 7913−7920

Comparison of the structure of [**Ru-1·C_2H_3**] with previously reported crystallographic data of [**Ru-1·C_2H_4**]$^+$ reveals a similar RuP_3S_3 core with clear distinctions associated with deprotonation at C55. Selected bond distances and angles are listed in Table 2. The Ru−P bond distances are shorter by 0.02−0.04 Å in [**Ru-1·C_2H_3**] relative to [**Ru-1·C_2H_4**]$^+$. Conversion of S3 from a thioether in [**Ru-1·C_2H_4**]$^+$ to a thiolate in [**Ru-1·C_2H_3**] results in a bond distance increase of 0.06 Å from 2.3365(9) to 2.3992(5) Å. There is also an increase in the Ru−S2 bond distance of 0.03 Å from 2.3749(9) to 2.4014(5) Å. The C55−C56 bond distance decreases from 1.510(5) to 1.313(4) Å, consistent with formation of a C═C double bond, confirming deprotonation of dithioether. Cleavage of the 5-membered Ru−S2−C55−C56−S3 ring upon deprotonation opens the Ru−S2−C55 bond angle from 104.52(12)° in [**Ru-1·C_2H_4**]$^+$ to 112.23(8)° in [**Ru-1·C_2H_3**]. Deprotonation also allows expansion of the S1−Ru−S2 and S1−Ru−S3 bond angles from 87.06(3)° to 95.030(18)° and 173.73(3)° to 178.19(2)°, respectively.

NMR Investigations. The dithioether complex [**Ru-1·C_2H_4**]$^+$, its monodeuterated derivative [**Ru-1·C_2H_3D**]$^+$, and the vinyl metallosulfonium complex [**Ru-1·C_2H_3**] have been thoroughly characterized by NMR techniques. A summary of pertinent ^{1}H, ^{13}C, and ^{31}P chemical shift values and coupling constants are summarized in Table 3.

The ^{1}H NMR spectrum of [**Ru-1·C_2H_4**]$^+$ displays four unique resonances for the ethylene bridge assigned as H1 (1.29, td), H2 (3.03, dd), H3 (1.59, td), and H4 (2.78, dd). The pseudoaxial protons H1 and H3 are located upfield with respect to the pseudoequatorial protons H2 and H4. gCOSY NMR, Figure S6, Supporting Information, clearly shows the coupling between four ethylene protons. The coupling constants are J_{13} = 14 Hz, $J_{12} \approx J_{34}$ = 14 Hz, $J_{14} \approx J_{23}$ = 4 Hz, and $J_{24} \approx 0$ Hz. The aromatic region between δ = 6.2 and 8.5 exhibits a complex multiplet of peaks associated with the nine phenyl rings and a total integration proportional to the four ethylene protons. The ^{31}P NMR spectrum of [**Ru-1·C_2H_4**]$^+$ is second order with chemical shifts and coupling constants as previously reported,[20] see Table 3. The ^{13}C NMR of [**Ru-1·C_2H_4**]$^+$ shows the ethylene carbons C55 (36.0, s) and C56 (44.2, s) along with nine phenyl rings carbons in region of δ = 110−180 ppm.

Substitution of a single ethylene proton by deuterium, as shown in Scheme 2, occurs selectively at the pseudoequatorial position on C55, H4. The ^{1}H NMR of [**Ru-1·C_2H_3D**]$^+$ displays three of the resonances associated with the ethylene bridge in [**Ru-1·C_2H_4**]$^+$ (H1 (1.29, t); H2 (3.03, dd); H3 (1.59, dd)) with the peak at δ = 2.78 ppm notably absent. The presence of deuterium at the pseudoequatorial position on C55 is further confirmed by gCOSY NMR, Figure S9, Supporting Information, which clearly shows the expected coupling pattern. The ^{13}C NMR of [**Ru-1·C_2H_3D**]$^+$ also confirms the selective deuterium labeling at C55 with a slight upfield shift of the peak to δ = 35.8 ppm and a coupling constant of 20.4 Hz. Deuteration at C55 has no effect on the ^{31}P NMR spectrum of [**Ru-1·C_2H_3D**]$^+$.

The NMR spectra of [**Ru-1·C_2H_3**] are complicated by a fluxional process associated with the vinyl substituent. At low temperature, ^{31}P NMR shows two partially overlapping second-order spectra, Figure 3. The first isomer (53%) has chemical shifts values for P1, P2, and P3 of δ = 65.6, 50.8, and 57.8 ppm, respectively, with coupling constants J_{12} = 303 Hz, $J_{13} = J_{23}$ = 30 Hz. In the second component (47%) the chemical shifts of P1 and P2 are significantly upfield at δ = 48.9 and 44.5 ppm. The P3 resonance, δ = 57.9 ppm, and the coupling constants, J_{12} = 299 Hz and $J_{13} = J_{23}$ = 32 Hz, are similar to the first isomer. As the temperature is increased, the two sets of resonances begin to converge with coalescence occurring at 303 K. At higher temperatures, a single set of resonances is observed, Figure 3 and Table 3.

Fluxional behavior of the vinyl substituent in [**Ru-1·C_2H_3**] is also observed in the ^{1}H NMR, Figure S11, Supporting Information. As detailed in the Computational Studies section below, this is attributed to lone-pair inversion at the vinyl metallosulfonium sulfur. At low temperature (223 K), one set of vinyl resonances is clearly visible with chemical shift values of

Table 3. Selected NMR Parameters for [Ru-1·C_2H_4]$^+$, [Ru-1·C_2H_3D]$^+$, and [Ru-1·C_2H_3] (δ, ppm; J, Hertz)

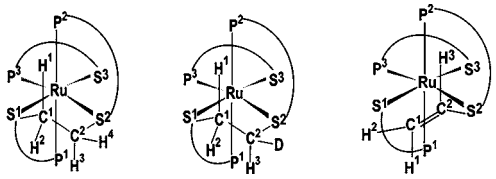

^{1}H NMR					
H1	1.29 (1H, td)	H1	1.29 (1H, t)	H1[a]	4.01 (1H, d)
H2	3.03 (1H, dd)	H2	3.03 (1H, dd)	H2[a]	4.40 (1H, d)
H3	1.59 (1H, td)	H3	1.59 (1H, dd)	H3[a]	4.94 (1H, dd)
H4	2.78 (1H, dd)	$J_{13} = J_{12}$ = 14 Hz		J_{13}[a] = 16 Hz	
$J_{13} = J_{12} = J_{34}$ = 14 Hz		J_{23} = 4 Hz		J_{23}[a] = 9 Hz	
$J_{14} = J_{23}$ = 4 Hz					
^{13}C NMR					
C1	44.2 (s)	C1	44.2 (s)	C1[b]	120 (s)
C2	36.2 (s)	C2	35.8 (t)		
		J_{C2D} = 20.4 Hz			
^{31}P NMR					
P1[c]	40.3[e]	P1	40.3[e]	P1[d]	55.4[e]
P2[c]	37.5[e]	P2	37.5[e]	P2[d]	48.7[e]
P3[c]	61.0[e]	P3	61.0[e]	P3[d]	58.3[e]
J_{12}[c] = 304 Hz		J_{12} = 304 Hz		J_{12}[d] = 310 Hz	
J_{13}[c] = J_{23} = 30 Hz		$J_{13} = J_{23}$ = 30 Hz		$J_{13} = J_{23}$[d] = 30 Hz	

[a]Resonances for one of two isomers observed at 223 K. Peaks associated with the other isomer are obscured by the phenyl resonances. [b]Recorded at 343 K. [c]Reference 20. [d]Recorded at 363 K. [e]Second-order spectrum (see text).

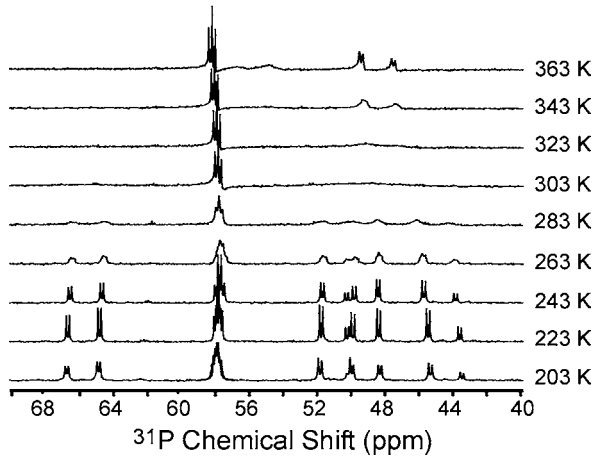

Figure 3. Variable-temperature ^{31}P NMR spectra of [**Ru-1·C_2H_3**].

dx.doi.org/10.1021/ic300983x | Inorg. Chem. 2012, 51, 7913−7920

δ = 4.01, 4.40, and 4.94 ppm for H1, H2, and H3, respectively. The coupling between the three resonances is confirmed by gCOSY NMR, Figure S12, Supporting Information. The second set of vinyl resonances is hidden in the aromatic region. As in the ^{31}P NMR, coalescence is observed upon an increase in temperature followed by a single set of resonances at higher temperatures, Table 3 and Figure S11, Supporting Information. The first set of resonances is further upfield than the chemical shift range from δ = 4.7 to 6.6 ppm observed in other vinyl metallosulfonium complexes.[2−6] This is consistent with shielding effects of the aromatic diphenyl substituents of the ligand. As suggested by a reviewer, the upfield shift of the vinyl protons could also be due to a linkage isomer with an η^2-coordinated vinyl substituent. While we cannot completely discount this possibility, similar Ru complexes display proton resonances in the range from δ = 1.3 to 3.0 ppm,[38] which is significantly further upfield than that observed in [**Ru-1**·C_2H_3].

From the variable-temperature ^{31}P NMR data, the activation barrier associated with the fluxional process was calculated as 13.08 kcal/mol.[39] Several possible origins of the fluxional process were considered including vinyl group transfer between S2 and S3, rotation of the vinyl substituent about the S2−C55 bond axis, and lone-pair inversion at S2. To discriminate between these possibilities, a series of DFT investigations was conducted.

Computational Studies. The B3LYP exchange-correlation functional with the LANL2DZ basis set was used for Ru and the 6-31g basis set for all other atoms to optimize the structure of [**Ru-1**·C_2H_3] and its derivatives. The calculated metal−ligand bond distances reproduce the experimental values for [**Ru-1**·C_2H_3] within 0.11−0.14 Å, Table 2. Calculated bond angles reproduce experimental values within 2−3°, Table 2.

Inversion of the S2 lone pair was modeled by systematic variation of the Ru−S2−C19−C55 torsion angle, Figure 4. In the X-ray crystal structure this angle is observed as −116.06°, which corresponds with the calculated minimum of −115.6°. A second minimum is observed near +120° as expected for a lone-pair inversion on S2. The energy barrier between these two minima of 14.36 kcal/mol is close to the measured activation barrier, 13.08 kcal/mol, for the fluxional process by

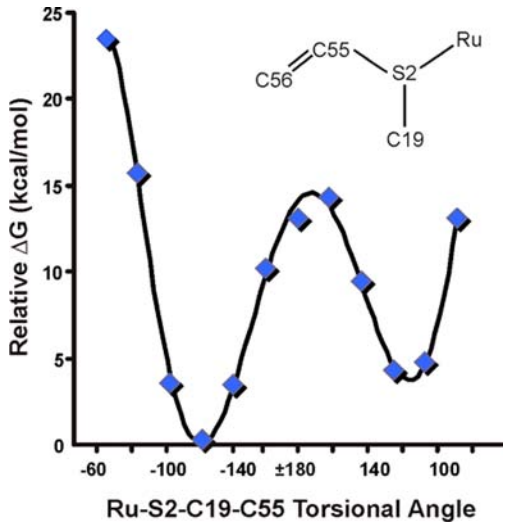

Figure 4. Calculated relative free energies of [**Ru-1**·C_2H_3] as a function of the Ru−S2−C19−C55 torsion angle representative of a sulfur lone-pair inversion at S2.

^{31}P NMR. The barrier is also consistent with previously reported sulfur lone pair inversions in metal thioether complexes,[40−42] which display inversion barriers less than those typically observed in pyramidal sulfoniums, ∼27−30 kcal/mol,[43] and significantly lower than comparable sulfoxides.[44] An alternate fluxional process attributed to rotation of the vinyl substituent about the S2−C55 bond angle has too low of an activation barrier, 4.38 kcal/mol (Figure S4, Supporting Information), to be considered.

A third potential fluxional process involves vinyl group transfer between S2 and S3. However, this is readily negated by energy calculations. The optimized structure of the crystallographically observed isomer with the vinyl group on S2 (trans to P3) is stabilized by 6.78 kcal/mol relative to the isomer with the vinyl substituent on S3 (trans to S1). This difference in thermodynamic energies is too large to observe the disfavored isomer in the ^{31}P NMR spectra regardless of the associated kinetic barrier (not calculated).

A comparison of the two optimized structural isomers reveals a more crowded steric environment for the vinyl group when it is on S3 as compared to S2. To quantify the steric versus electronic effects, truncated computational models of each isomer with the diphenyl substituents of the DPPBT ligand replaced with methyl (DMPBT) or hydrogen (PBT) were calculated, Table 4. The results show a consistent preference for

Table 4. Calculated Relative Energies of Vinyl Metallosulfonium Complexes with the Substituent on the Sulfur Trans to Sulfur (tS) or Trans to Phosphorus (tP) for [Ru-1·C_2H_3] (left) and Its Truncated Derivatives [$(DMPBT)_2$(DMPBT·C_2H_3)Ru] (center) and [$(PBT)_2$(PBT·C_2H_3)Ru] (right)[a]

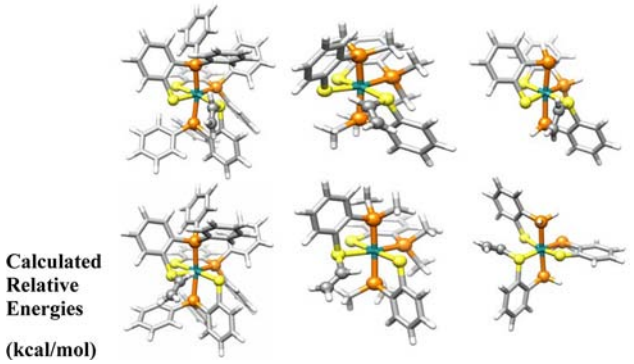

$\Delta H_{tS} - \Delta H_{tP}$	6.36	3.21	4.03
$T\Delta S_{tS} - T\Delta S_{tP}$	−0.43	−1.74	0.19
$\Delta G_{tS} - \Delta G_{tP}$	6.78	4.95	3.83

[a]DMPBT = dimethylphosphinebenzenethiolate, PBT = phosphinebenzenethiolate.

the vinyl group on S2 relative to S3, although the energy gap decreases with decreased steric bulk on the ligand. While the steric contribution may facilitate formation of one isomer over the other, clearly electronic effects are significant in dictating the position of the vinyl group on the sulfur trans to P as opposed to trans to S. Efforts to prepare these less sterically hindered derivatives are underway.

■ CONCLUSIONS

In this study we have shown that thioether coordination to a metal center may impart "sulfonium-like" ligand-centered

dx.doi.org/10.1021/ic300983x | Inorg. Chem. 2012, 51, 7913−7920

reactivity such as base-induced eliminations. These complexes can be considered as metalloderivatives of trialkyl sulfoniums or metallosulfoniums. The cationic metal−dithioether complex $[\mathbf{Ru\text{-}1{\cdot}C_2H_4}]^+$ has a five-membered MS_2C_2 ring that has been shown to be particularly base sensitive in related complexes. The ring contains four hydrogen atoms (H1, H2, H3, and H4) as potential sites for deprotonation, Figure 5. The two

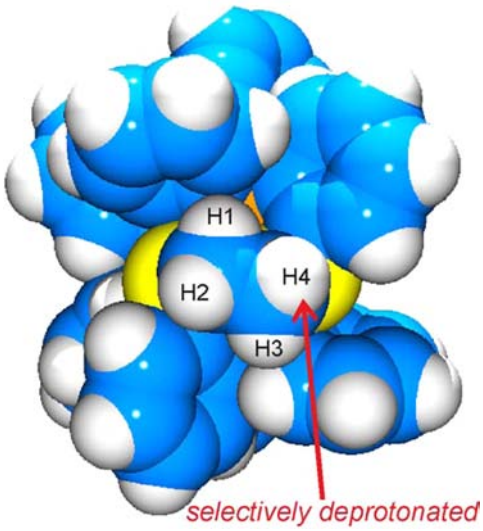

Figure 5. Space-filling model of $[\mathbf{Ru\text{-}1{\cdot}C_2H_4}]^+$ showing the site of selective deprotonation at the pseudoequatorial site H4.

pseudoaxial protons (H1, H3) are directed toward the phenyl substituents of the PS chelates and thus are sterically crowded. The equatorial protons (H2 and H4) are more sterically accessible and thus more susceptible to deprotonation. Of these, the H4 proton is selectively removed, generating the vinyl metallosulfonium complex $[\mathbf{Ru\text{-}1{\cdot}C_2H_3}]$ with the vinyl substituent on the sulfur trans to the π-accepting phosphine. Through DFT calculations we have shown deprotonation to yield this structural isomer to be enthalpically driven.

Reprotonation of $[\mathbf{Ru\text{-}1{\cdot}C_2H_3}]$ under acidic conditions also is a selective process as demonstrated by deuterium-labeling studies. In contrast to vinyl sulfides ($RSCH{=}CH_2$) which are typically considered to be "electron-rich" alkenes, vinyl sulfoniums ($R_2S^+CH{=}CH_2$) are "electron poor" and subject to nucleophilic attack. Metal coordination extracts electron density from the sulfur, imparting vinyl metallosulfonium character on the substituent group. We tentatively attribute the selectivity of the reprotonation reaction to nucleophilic attack by the *cis*-thiolate donor at the β-carbon of the vinyl group followed by rapid protonation of the resulting carbanion at the α position. Further studies to detail the mechanistic pathway and extend the observed ligand center reactivity to other $[\mathbf{Ru\text{-}1{\cdot}alkene}]^+$ derivatives with substituted alkenes are underway.

■ ASSOCIATED CONTENT

Supporting Information

+ESI-MS and NMR spectra of $[\mathbf{Ru\text{-}1{\cdot}C_2H_4}]^+$, $[\mathbf{Ru\text{-}1{\cdot}C_2H_3}]$, and $[\mathbf{Ru\text{-}1{\cdot}C_2H_3D}]$, cyclic voltammogram of $[\mathbf{Ru\text{-}1{\cdot}C_2H_3}]$, and optimized Cartesian coordinates in pdf format, and crystallographic data for $[\mathbf{Ru\text{-}1{\cdot}C_2H_3}]$ in CIF format (CCDC 881016). This material is available free of charge via the Internet at http://pubs.acs.org.

■ AUTHOR INFORMATION

Corresponding Author

*E-mail: grapperhaus@louisville.edu.

Notes

The authors declare no competing financial interest.

■ ACKNOWLEDGMENTS

We thank the Donors of the American Chemical Society Petroleum Research Fund (51566-ND3) for support of this work. We thank the Kentucky Research Challenge Trust Fund for the purchase of CCD X-ray equipment and upgrade of our X-ray facility.

■ REFERENCES

(1) Knipe, A. C. In *The Chemistry of the Sulphonium Group, Part 1*; Stirling, C. J. M., Patai, S., Eds.; John Wiley & Sons: Chichester, 1981; pp 334−347.
(2) Singh, A. K.; Mukherjee, R. *Dalton Trans.* **2008**, 260−270.
(3) Blake, A. J.; Holder, A. J.; Hyde, T. I.; Kuppers, H. J.; Schroder, M.; Stotzel, S.; Wieghardt, K. *J. Chem. Soc., Chem. Commun.* **1989**, 1600−1602.
(4) Bennett, M. A.; Goh, L. Y.; Willis, A. C. *J. Am. Chem. Soc.* **1996**, *118*, 4984−4992.
(5) Shin, R. Y. C.; Tan, G. K.; Koh, L. L.; Goh, L. Y. *Organometallics* **2004**, *23*, 6293−6298.
(6) Sellmann, D.; Barth, I.; Knoch, F.; Moll, M. *Inorg. Chem.* **1990**, *29*, 1822−1826.
(7) Walling, C.; Helmreich, W. *J. Am. Chem. Soc.* **1958**, *81*, 1144−1148.
(8) Chatgilialoglu, C.; Ferreri, C.; Ballestri, M.; Mulazzani, Q. G.; Landi, L. *J. Am. Chem. Soc.* **2000**, *122*, 4593−4601.
(9) Ichinose, Y.; Oshima, K.; Utimoto, K. *Chem. Lett.* **1988**, 669−672.
(10) Lalevee, J.; Allonas, X.; Fouassier, J. P. *J. Org. Chem.* **2006**, *71*, 9723−9727.
(11) Wang, K.; Stiefel, E. I. *Science* **2001**, *291*, 106−109.
(12) Wing, R. M.; Tustin, G. C.; Okamura, W. H. *J. Am. Chem. Soc.* **1970**, *92*, 1935−1939.
(13) Dang, L.; Shibl, M. F.; Yang, X.; Alak, A.; Harrison, D. J.; Fekl, U.; Brothers, E. N.; Hall, M. B. *J. Am. Chem. Soc.* **2012**, *134*, 4481−4484.
(14) Harrison, D. J.; Lough, A. J.; Nguyen, N.; Fekl, U. *Angew. Chem., Int. Ed.* **2007**, *46*, 7644−7647.
(15) Harrison, D. J.; Nguyen, N.; Lough, A. J.; Fekl, U. *J. Am. Chem. Soc.* **2006**, *128*, 11026−11027.
(16) Kerr, M. J.; Harrison, D. J.; Lough, A. J.; Fekl, U. *Inorg. Chem.* **2009**, *48*, 9043−9045.
(17) Ouch, K.; Mashuta, M. S.; Grapperhaus Craig, A. *Eur. J. Inorg. Chem.* **2012**, 475−478.
(18) Ouch, K.; Mashuta, M. S.; Grapperhaus, C. A. *Inorg. Chem.* **2011**, *50*, 9904−9914.
(19) Grapperhaus, C. A.; Ouch, K.; Mashuta, M. S. *J. Am. Chem. Soc.* **2009**, *131*, 64−65.
(20) Grapperhaus, C. A.; Venna, K. B.; Mashuta, M. S. *Inorg. Chem.* **2007**, *46*, 8044−8050.
(21) Grapperhaus, C. A.; Kozlowski, P. M.; Kumar, D.; Frye, H. N.; Venna, K. B.; Poturovic, S. *Angew. Chem., Int. Ed.* **2007**, *46*, 4085−4088.
(22) Shin, R. Y. C.; Teo, M. E.; Leong, W. K.; Vittal, J. J.; Yip, J. H. K.; Goh, L. Y.; Webster, R. D. *Organometallics* **2005**, *24*, 1483−1494.
(23) Grapperhaus, C. A.; Poturovic, S. *Inorg. Chem.* **2004**, *43*, 3292−3298.
(24) Poturovic, S.; Grapperhaus, C. A.; Mashuta, M. S. *Angew. Chem., Int. Ed.* **2005**, *44*, 1883−1887.
(25) Dilworth, J.; Zheng, Y.; Lu, S.; Wu, Q. *Transition Met. Chem.* **1992**, *17*, 364−368.

(26) Sandström, J. *Dynamic NMR Spectroscopy*; Academic Press: London, 1983.
(27) *CrysAlis PRO (CCD and RED)*, V 171.35.11; Oxford Diffraction Ltd.: Yarnton, England, 2011.
(28) SCALE3 ABSPACK included in CrysAlis PRO RED, V 171.35.11,
(29) Sheldrick, G. M. *Acta Crystallogr.* **2008**, *A64*, 112−122.
(30) *SHELXTL v6.14, Program Library for Structure Solution and Molecular Graphics*; Bruker Advanced X-ray Solutions, Inc.: Madison, WI, 2000.
(31) *Gaussian 09*, revision C.02; Gaussian, Inc.: Wallingford, CT, 2009.
(32) Sawyer, D. T.; Roberts, J. L. *Acc. Chem. Res.* **1988**, *21*, 469−476.
(33) Sawyer, D. T.; Sobkowiak, A.; Roberts, J. L. *Electrochemistry for Chemists*, 2nd ed.; John Wiley & Sons, Inc.: New York, 1995.
(34) Farmer, P. J.; Reibenspies, J. H.; Lindahl, P. A.; Darensbourg, M. Y. *J. Am. Chem. Soc.* **1993**, *115*, 4665−4674.
(35) Grapperhaus, C. A.; Poturovic, S.; Mashuta, M. S. *Inorg. Chem.* **2005**, *44*, 8185−8187.
(36) Farrugia, L. J. *J. Appl. Crystallogr.* **1997**, *30*, 565.
(37) Pérez-Lourido, P.; Romero, J.; García-Vázquez, J. A.; Castro, J.; Sousa, A.; Cooper, L.; Dilworth, J. R.; Richards, R. L.; Zheng, Y.; Zubieta, J. A. *Inorg. Chim. Acta* **2003**, *356*, 193−202.
(38) Planas, J. G.; Marumo, T.; Ichikawa, Y.; Hirano, M.; Komiya, S. *J. Chem. Soc., Dalton Trans.* **2000**, 2613−2625.
(39) Zimmer, K. D.; Shoemaker, R.; Ruminski, R. R. *Inorg. Chim. Acta* **2006**, *359*, 1478−1484.
(40) Adams, H.; Amado, A. M.; Félix, V.; Mann, B. E.; Antelo-Martinez, J.; Newell, M.; Ribeiro-Claro, P. J. A.; Spey, S. E.; Thomas, J. A. *Chem.—Eur. J.* **2005**, *11*, 2031−2046.
(41) Baradello, L.; Lo Schiavo, S.; Nicolò, F.; Lanza, S.; Alibrandi, G.; Tresoldi, G. *Eur. J. Inorg. Chem.* **2004**, *2004*, 3358−3369.
(42) Tresoldi, G.; Lo Schiavo, S.; Lanza, S.; Cardiano, P. *Eur. J. Inorg. Chem.* **2002**, *2002*, 181−191.
(43) Wiegrefe, A.; Brinkmann, T.; Uzar, H. C. *J. Phys. Org. Chem.* **2001**, *14*, 205−209.
(44) Scartazzini, R.; Mislow, K. *Tetrahedron Lett.* **1967**, *8*, 2719−2722.